2023 IEEE International Conference on Robotics and Automation (ICRA 2023)
May 29 - June 2, 2023. London, UK

A Flexible 3D Force Sensor with In-Situ Tunable Sensitivity

James Davies[1], Mai Thanh Thai[1], Trung Thien Hoang[1], Chi Cong Nguyen[1], Phuoc Thien Phan[1], Kefan Zhu[1], Dang Bao Nhi Tran[2], Van Anh Ho[3], Hung Manh La[4], Quang Phuc Ha[5], Nigel Hamilton Lovell[1], and Thanh Nho Do[1]

***Abstract*— Following biology's lead, soft robotics has emerged as a perfect candidate for actuation within complex environments. While soft actuation has been developed intensively over the last few decades, soft sensing has so far slowed to catch up. A largely unresearched area is the change of the soft material properties through prestress to achieve a degree of mechanical sensitivity tunability within soft sensors. Here, a new 3D force sensor which employs novel hydraulic filament artificial muscles capable of in-situ sensitivity tunability is introduced. Using a neural network (NN) model, the new soft 3D sensor can precisely detect external forces based on the change of the hydraulic pressures with error of ~1.0, ~1.3, and ~0.94 % in the x, y, and z-axis directions, respectively. The sensor is also able to sense large force ranges, comparable to other similar sensors available in the literature. The sensor is then integrated into a soft robotic surgical arm for monitoring the tool-tissue interaction during an ablation process.**

I. Introduction

While more numerous than their soft counterparts, hard robotic systems necessitate precise control systems and greater complexity with increasingly complex environments [1]. This, coupled with their troubled human interactions, is building the case for the increasing development in soft robotic systems [2, 3]. Following the success of biology in employing compliant materials and structures, soft robots are inherently flexible [2-4], which allows for self-regulating adaption to complex environments without complex control systems [2]. Compliance also means interactions with humans are inherently safe.

While there has been significant progress in the development of new soft actuators, there has been comparatively little attention towards the development of advanced soft sensing systems. Naturally, a compliant actuator requires a compliant sensing method, meaning most conventional sensors are inappropriate [3]. A new class of sensors are being developed that can be integrated into soft systems, including the human body [5]. An ideal soft sensor should have a greater operational strain than the objects in which it is integrated, and a low elastic modulus, both of which implies little resistance to the object's motion [6]. Such an ideal sensor is in great demand for healthcare applications such as prostheses, rehabilitation aids, and surgical systems, to provide closed loop control or display the contact information for safe operation.

There has been a large amount of work done to develop sensors such as resistive [7-18] or capacitive [19-22] ones. Recent progress has brought forward the development of new sensing mechanism including fluid pressure-based soft sensors, which have disproportionately targeted pneumatic pressure [6, 23-30]. The basic working principle behind these pressure-based fluidic soft sensors is the deformation of compliant fluid chambers, which alters the internal fluid's pressure. These soft sensors employ commercial fluid pressure sensors to monitor pressure changes. A small number of research groups have attempted to use this fluidic transduction method to create 3D or multi-axial force sensors. One example of such a sensor comes in the work done by Choi et al. [27], who created a three-axis force sensor whose working principle relies on three pneumatic chambers equally radially placed around a force post, all embedded in silicone layers. When an external force is applied to the post, it deforms the pneumatic chambers in the direction of the force, resulting in a change of the internal pressure. It takes the form of a disk with a 40 mm diameter and 10 mm thickness. In its current form, the device is not entirely scalable and is restricted by relatively large commercial pressure sensors. This scalability limitation means integrating a sensor such as this into small-scale applications, like surgical devices, is not possible. In this way, it is confined to larger scale applications such as those in wearable soft systems. While the fabrication of this sensor is not overly complex, it still requires a relatively lengthy molding, component insertion, and sealing process. This sensor exhibits a large degree of hysteresis, and compensates for this output variability using a filter, reducing its root-

This work was supported by UNSW Grant PS58173, UNSW Scientia Fellowship PS46197, Vanguard Grant from Heart Foundation RG204224.

[1]The authors are with the Graduate School of Biomedical Engineering, Faculty of Engineering, UNSW Sydney, Kensington Campus, NSW 2052, Australia (email: j.j.davies@student.unsw.edu.au, maithanh.thai@unsw.edu.au, trungthien.hoang@unsw.edu.au, cong.c.nguyen@unsw.edu.au, phuoc_thien.phan@unsw.edu.au, kefan.zhu@student.unsw.edu.au, n.lovell@unsw.edu.au, and tn.do@unsw.edu.au).

[2]The author is with the School of Science, Engineering & Technology, RMIT University, Vietnam Campus, Ho Chi Minh City, Vietnam (email: s3751881@rmit.edu.vn).

[3]The author is with the School of Material Science, Japan Advanced Institute of Science, and Technology (JAIST), Ishikawa, Japan Science and Technology Agency, PRESTO, Kawaguchi Saitama, Japan (email: van-ho@jaist.ac.jp).

[4]The author is with the Department of Computer Science and Engineering, University of Nevada, Reno, Reno, NV 89557 USA (email: hla@unr.edu).

[5]The author is with the Faculty of Engineering and IT, University of Technology Sydney, NSW 2007, Australia (email: Quang.Ha@uts.edu.au).

*Corresponding author: T. N. Do (tn.do@unsw.edu.au)

mean-squared non-linearity from 2.7% to 1.5%. The measured errors when compared with commercial sensors in the x, y, and z axis were 2.77, 4.11, and 1.62%, respectively. The sensor is capable of sensing up to 13 N in the z-axis and between -2.5 and 2.5 N in the x-axis. Other non-fluidic 3D force sensors have been developed, including magnetic-hall-effect sensors [31], liquid metal sensors [32], and piezoelectric sensors [33]. These three-axis sensors produce measured errors ranging from 4 – 17%.

Choi's work is one of the only fluidic 3D force sensors reported in the literature, but much more common are 1D fluidic force sensors. One such sensor, from the work of He et al. [34], utilized silicone air chamber structure as sensing element. Taking the form of a hollow silicone ball, this sensor used a commercial pressure sensor to monitor the changes in air pressure due to force. By changing the initial air pressure within the hollow dome, the air's response to external force changes too. Increasing the dome's initial pressure naturally inflates the structure and increases its stiffness. In this way, increasing the initial pressure increases the force required to deform the dome, and therefore decreases the sensitivity to force. This ability to alter sensitivity throughout operation gives this sensor a clear advantage over others for a great deal of applications.

Further, we have only been unable to identify a few hydraulic-based fluidic force sensors in the literature [35, 36], none of which have taken the form of 3D force sensors. While air introduces a degree of compliance to soft systems, it also introduces non-linearities due to its compressibility [37]. Hydraulic fluids, such as water or oil, are incompressible and are therefore far more linear in their response and more energy efficient, and therefore more sensitive [37-39]. Hydraulic systems are more reactive to load variations and respond 50 times faster than pneumatics, which is a major advantage in a sensor [37, 39-41].

In this paper, we present a 3D force sensor, based on a novel soft, strain/force sensing filament, which is capable of tuning its sensitivity in-situ to adapt to changes in contacting environments. The sensing filaments sense external force or strain through hydraulic transduction, and their novel tunability mechanism utilises the initial pressure of this hydraulic fluid (water). The 3D force sensor is manufactured using simple means, with no molding required, only 3D printing and gluing/adhesion. It is scalable, including its sensing filaments, meaning integration into smaller or larger applications is feasible. The proposed sensor is characterised by firstly examining the tunability capabilities of the individual sensing filaments, then the response of the 3D force sensor is investigated. Two calibration methods are presented, including a manual compensation method and a neural network (NN) driven, automated process. The device's application is then demonstrated in a surgical setting. The proposed sensor contributes positively to the development of mechanically tunable sensors, which have the potential to reduce the proportion of noise in a given signal when amplified.

II. Design and Fabrication

A. Working Principle

The key element of this 3D force sensor is the soft filament sensor (SFS), three of which form an equilateral triangular pyramid inside the sensor housing. Fig. 1a shows the structure and working principle of the SFS fibre. It consists of an inner elastomeric (silicone) tube inserted into the hollow channel of an outer spring coil. The inner tube is firstly pressurised to reach P_0 using water from a hydraulic pressure source (e.g., syringe). This pressurised state is defined as the resting state of the fibre where the hydraulic pressure stresses the walls of the inner silicone tube. Due to water's incompressibility, when the sensor fibre is stretched, the volume within the tube must stay constant. Therefore, if the sensor fibre is stretched axially, the inner radius of the tube must decrease to compensate for its increasing length. This effectively increases the thickness of the tube's walls and relieves the stress in those walls. This stress reduction due to axial stretching directly reduces the pressure in the water to a smaller value $P_i < P_0$. The sensor's water pressure is measured using a commercial pressure sensor via a fluid transmission tube.

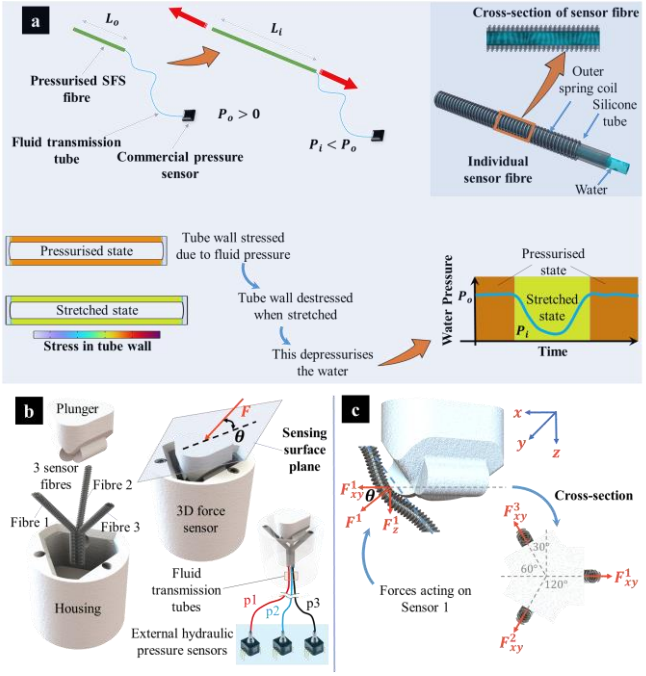

Figure 1. Design and working principle of the 3D force sensor. a) Design and working principle of the sensor fibres. b) Exploded, collapsed, and transparent views of the sensor with soft muscle fibres connected to external hydraulic pressure sensor. c) Detailed diagram of the components of forces acting on each sensor fibre.

While this method of transducing force is novel, the true innovation of this sensor fibre lies in its ability to tune its sensitivity to strain or applied force, which can adapt to different environments. As will be discussed in subsequent sections, altering the initial pressure at resting state alters the

rate of change of stress reduction within the tube's walls for some constant strain. Therefore, we can tune the rate of change of pressure drop within the water in response to this strain. Put simply, we can tune the gauge factor (GF) of each sensor fibre by altering its initial water pressure.

To transduce 3D force using these SFS fibres, we employ three in an equilateral triangular pyramid arrangement, supported by a 3D printed PLA housing. As shown in Fig. 1c, these three SFS fibres are routed through holes in the housing, with a central hole in its base accommodating all three fibres and their respective fluid transmission tubes. A 3D printed PLA plunger is placed on the exposed segments of all three sensors, which forms the sensing surface of the 3D force sensor. As seen in Fig. 1b, when a force is applied to the plunger, it will deform the sensors below. This deformation applies a degree of axial strain on each SFS fibre, which leads to a corresponding drop in their respective hydraulic pressure signals. We then apply a mathematical formula to decode the *x*, *y*, and *z* components of the applied force *F* from the three SFS fibre signals. Below is the system of equations used to translate each sensor signal into 3-dimensional force, where *N=1, 2, 3* is the sensor number (fibre 1, fibre 2, fibre 3, Fig. 1c) and θ is the acute angle made by each sensor fibre and the sensing surface plane, as shown in Figs. 1b and 1c.

$$F_{xy}^{N} = F^{N}\cos\theta \tag{1}$$

$$F_{z}^{N} = F^{N}\sin\theta \tag{2}$$

$$\begin{bmatrix} F_x \\ F_y \\ F_z \end{bmatrix} = \begin{bmatrix} F_{xy}^{1} - \left(F_{xy}^{2} + F_{xy}^{3}\right)\cos 60^{\circ} \\ \left(F_{xy}^{3} - F_{xy}^{2}\right)\cos 30^{\circ} \\ F_{z}^{1} + F_{z}^{2} + F_{z}^{3} \end{bmatrix} \tag{3}$$

B. Fabrication

Beginning with the SFS fibres, a detailed fabrication process can be found in our recent works [42, 43]. While our previous work describes this structure as a soft actuator, here we are using it as a soft sensor where the working principle is completely different. Briefly, the silicone inner silicone tube was sourced from Saint-Gobain S.A. (Courbevoie, France), and the outer spring coil was sourced from ASAHI Intecc Co., Ltd. (Japan). Both the housing and the plunger were manufactured using an Ultimaker 2+ 3D printer (Ultimaker B.V., Netherlands) with PLA (Ultimaker PLA, Ultimaker B.V., Netherlands).

The three fabricated SFS fibres are routed through the central, common hole in the housing and up into their respective anchoring holes in the rim of the housing. Each fibre is then fixed in these anchoring holes using adhesive glue (UHU GmbH & Co. KG). At this point, one end of each sensor is fixed to the housing, while the other end (the transmission tube end) is free in the central housing hole. The SFS fibres are then pressurised to the desired level, and their other end is fixed in the central housing hole using adhesive glue. This leaves the three transmission tubes free, while the sensors are fixed in the housing.

The plunger is then placed on top of the fibres and aligned within the housing, before the gap between the plunger and the housing is filled using Sil-Poxy (Smooth-On, Inc.). This fixes the plunger in its resting position, while the elastic Sil-Poxy allows it to return to this position after an applied force. The elastic modulus of this gap-filling adhesive governs the sensitivity of the plunger's movement in response to force. This completes the fabrication of the 3D force sensor. It is noted that the sensitivity of the sensor highly depends on the filled silicone. A softer silicone (e.g., Ecoflex-0030, Smooth-On, Inc.,) would certainly give a higher sensitivity. The investigation on the sensor performance with different silicone elastomers is out of scope of this paper and we leave it for the future work.

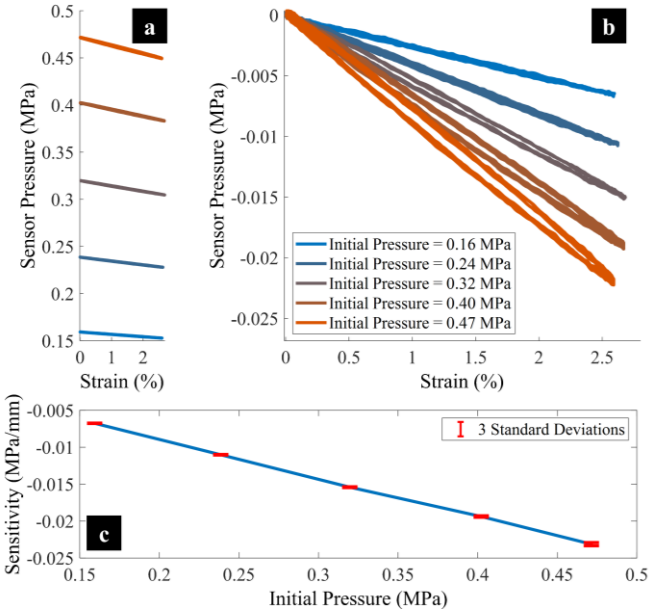

Figure 2. Sensitivity tunability of a straight SFS fibre. a) Unadjusted sensor pressure with respect to sensor strain at increasing initial sensor pressure. The sensor pressure value at zero strain was the initial pressure in the sensor. b) Adjusted sensor data from (a) where data from each initial pressure was shifted to zero. This allows for better visualization of the gradient of each initial pressure's response to strain. c) The sensitivity of the sensor with respect to initial pressure. This data was taken from the gradient of the line of best fit for each initial pressure response in (b).

III. Results and Discussion

A. SFS Fibre Tunability Characterisation

Table I details the component specifications for the characterisation of the SFS fibre tunability. This characterisation was performed on a straight fibre, which was stretched purely axially for the sake of simplicity. The fibre was connected to a syringe pressure source (BD Luer-Lok™), driven by a linear motor (model XLRQ150BL-E01, Zaber, Canada), and a pressure sensor (40PC Series Sensor, Honeywell, USA). The transmission tube end of the fibre was fixed in place, while the free end was attached to a Zaber linear motor. The movement of the linear motor was monitored using an encoder. The fibre was pressurised to a given initial pressure, and then elongated in a sinusoidal motion by the linear motor, while its pressure and elongation

was monitored. The sinusoidal motion has a peak of 1 mm, corresponding to a sensor strain of approximate 2.7%. This low strain was applied to mimic the low strains necessary for force sensing. Each test contained 5 elongation cycles and was repeated three times before the initial pressure was increased and the process was repeated.

Fig. 2 shows the results of this testing. Fig. 2a reveals the unadjusted pressure data with respect to elongation for each initial pressure. While Fig. 2b reveals the same data but with each initial pressure adjusted to zero, to better compare the difference in gradient between each initial pressure. Fig. 2c shows the fitted gradient of each of the sensor responses in Fig. 2b with respect to initial pressure. This is effectively a graph of the sensitivity (or gauge factor, GF) of the SFS fibre with respect to initial pressure. Fig. 2b suggests that the pressure drop is linear with respect to forced elongation, at least in this small strain range. There is increasing hysteresis as initial pressure increases, but the degree of hysteresis is still relatively low. Fig. 2c indicates that the sensitivity increases linearly with initial pressure, within the pressure range we tested.

TABLE I. SPECIFICATIONS FOR SFS FIBRE COMPONENTS

Component	Specifications
Inner tube	OD 1.19 mm, ID 0.635 mm, length 37 mm, silicone rubber
Outer coil	OD 1.49 mm, ID 1.10 mm, length 37 mm, stainless steel

The minimum sensitivity observed was -6.76 kPa/mm (with 159.37 kPa input pressure) while the maximum was -23.12 kPa/mm (with 471.42 kPa input pressure). Which corresponds to a maximum change in sensitivity of 16.36 kPa/mm with an increase in input pressure of 312.05 kPa.

This is of course an idealized scenario, and the dynamics within the 3D force sensor are more complicated than this purely linear, axial strain testing. However, this was carried out to present the capability of the sensor fibres in the clearest possible way.

TABLE II. SPECIFICATIONS FOR SFS FIBRE COMPONENTS

Component	Specifications
Inner tube	OD 0.610 mm, ID 0.305 mm, length 15 mm, silicone rubber
Outer coil	OD 0.800 mm, ID 0.600 mm, length 15 mm, stainless steel

B. 3D Force Sensor Manual Calibration

Having demonstrated the tunability of the single sensor fibre, we tested their use in the proposed 3D force sensor design. The specifications for the sensor fibres used in this testing can be found in Table II. The dimensions of these sensor fibres were reduced when compared with Table I such that we could manufacture a smaller 3D force sensor. The 3D force sensor was fabricated as described previously. The sensing surface of the 3D force sensor was fixed to the sensing surface of an ATI Nano17 6-axis force sensor (Calibration SI-25-0.25, ATI Industrial Automation, USA) using an adhesive glue. The 3D force sensor was clamped in place and the ATI was pushed onto the force sensor in various directions using human hands. This was done, instead of setting up a complicated rig, for simplicity, since the direction of applied force should not matter.

Fig. 3 shows the calibrated signal from the 3D force sensor alongside the ATI control data. While Fig. 3c reveals the two sensor's data plotted against each other, along with the root means square error (RMSE) of each dimension of force. The 3D force sensor data was calculated from the 3 SFS fibre signals using Eqs. (1), (2), and (3). After using these equations, the resultant directional force signals were manually calibrated by plotting the SFS pressure signal against the ATI data. Linear curve fitting gave the transformation between the raw force data and the calibrated force data.

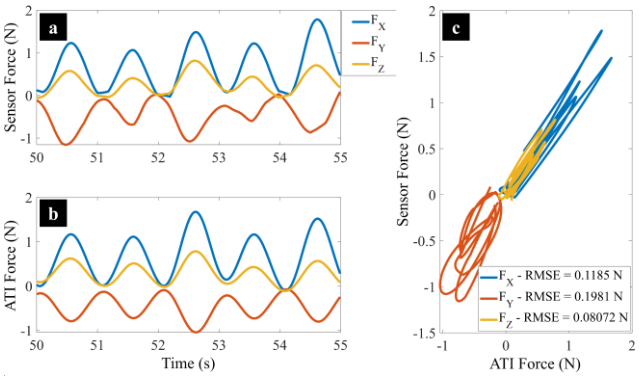

Figure 3. Calibrated force data from the 3D force sensor and ATI control. a) Calibrated x, y, and z axis force from the proposed sensor. b) x, y, and z axis force from the reference sensor (ATI Nano17). c) Proposed sensor *x, y,* and *z* axis force data plotted against the reference sensor data.

Fig. 3 shows a similar trend in both sensors' force data, but there are clear inconsistencies in the 3D force sensor's response. This is seen most obviously in the *y*-component of force, where large hysteresis and inconsistent loading and unloading is visible. The other two force directions behaved better, with low loading/unloading hysteresis, but some inconsistency between cycles evident. This instability in the response of the 3D sensor is likely due to inconsistent contact dynamics between the plunger and each SFS fibre. Given their high sensitivity, even slight changes in contact between loading cycles would produce a differently shaped output. The *x, y,* and *z*-axis errors demonstrated here were ~23, ~39, and ~16% respectively. Future work should include an attempt to stabilize the contact between the plunger and SFS fibres.

C. 3D Force Sensor Neural Network Calibration

With the potential of the 3D force sensor shown above, the challenge is to employ a method of intelligent calibration that can take the SFS pressure data directly and transform it into force data. To do this, we have used a neural network (NN) model. Such a technique of interpreting the sensor data

removes the need to manually process the data, which gives inconsistent results. Training a NN to interpret the data accounts for the idiosyncrasies of each sensor's contact dynamics, as described above. This can potentially reduce the large errors seen above when manually calibrating and diminish the effort to derive mathematical relations.

The NN approach (Fig. 4b) requires a sufficient amount of data to approximate the calibrated relationship between desired force data from the 3 Axis ATI force sensor and pressure data from our proposed force sensor. Therefore, the NN model was trained by datasets with pressure data (p1, p2, p3) as inputs and time-varying force value in *x, y,* and *z* axis as outputs. The datasets were collected by randomly applying force to both our proposed sensor and ATI force sensor with a sampling rate of 100 Hz using the experimental setup shown in Fig. 4a.

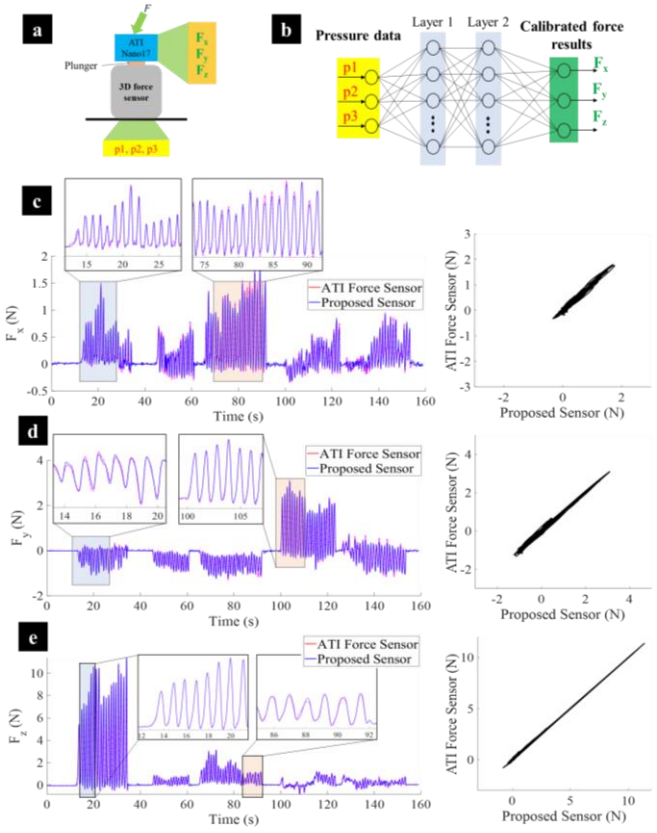

Figure 4. Architecture of a neural network (NN) model for intelligent calibration. a) Experiment setup for data collection. b) Overview of the NN calibration. c-e) Calibrated x, y, and z axis force from the proposed sensor (left panel) and the relationship against the 3 axis ATI force sensor (right panel).

Note that the trained force range is from -0.5 N to 2 N in *x*-axis, -1 N to 4 N in *y*-axis and -1 N to 11 N in *z*-axis to limit the datasets, which is sufficient for our intended applications. One thousand datasets were collected and randomly split into training/validation/testing sets in the ratio of 75/15/15, respectively. A neural network with two hidden layers and Bayesian Regularization backpropagation was applied to train the network parameters. The network was trained using the Dynamic Time-series function in MATLAB and ten delay samples with Intel Xeon E-2136 @ 3.30GHz. When implementing the trained NN to the real setup, current pressure in SFSs were continuously inputted to the trained model and the output signal was the force data in 3 axes. Note that this is an offline-learning controller and soft force sensor may change their characteristics over a long period of time, so a new data set is needed to retrain the model in future. The results given in Figs. 4c-e by applying the trained model to a data show that the measured errors when compared with the ATI Nano17 force sensor for *x, y*, and *z*-axis were ~1.0, ~1.3, and ~0.94% respectively. It can be seen that intelligent calibration with NN outperformed the manual calibration in soft force sensor where nonlinearity is prevalent. To achieve a higher accuracy in line with the repeatability of the force sensing device, a better NN model and more data sets should be used [44].

D. Application of 3D Force Sensor in a Surgical System

One of the main disadvantages of existing teleoperated robot-assisted minimally invasive surgery systems compared to open surgery is the lack of force sensing to provide the reaction force of the instruments to a surgeon during an operation [45]. In endoscopic submucosal dissection (ESD), dissection under an endoscope requires delicate skills, the implementation of a force-feedback system can improve the safety of the operation. In this work, we implemented the developed 3D force sensor into a tip of a soft robotic arm to sense the interaction force when performing palpation or tissue dissection in ESD. This was done to indicate the potential for the sensor's integration into surgical applications through future investigations and development.

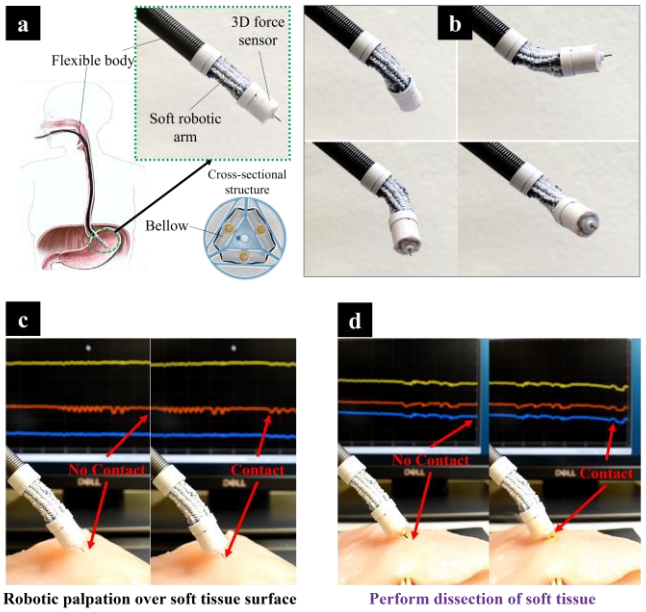

Figure 5. Demonstration experiment with a flexible robotic arm integrated with the 3D force sensor. a) The design and the potential use in the gastrointestinal tract. b) Cumulative image representing the bending motions of the 3D robotic arm. c) Robotic palpation of soft tissue without touching (left panel) and touching (right panel). d) Robotic dissecting soft tissue without touching (left panel) and touching (right panel).

The 3-DOF soft robotic arm was fabricated by combining three soft wrinkled fabric bellows in parallel and at the

vertices of an equilateral triangle to create omnidirectional motions at the tip (Fig. 5a). The bending movement of the arm is regulated by hydraulic pressures inside the bellows which is transmitted from external linear hydraulic units via micro-sized PTFE tubes (Cole-Parmer, USA). Energizing a single bellow will produce bending movement in one direction while actuation of two bellows causes bending movement in the plane in between the two bellows. Similarly, when all three bellows simultaneously receive the same hydraulic pressure, a linear translational motion is achieved along its long axis. It means that the soft robotic arm can extend its length without moving the flexible body, which is critical for most cables-driven surgical robots where external translation motion is required. The fluid transmission tubes for the 3D force sensor and electrical wire for electrosurgery are routed along a central channel of the robotic arm to minimize the system's overall size. Fig. 5b represents various motions of the soft robotic arm when bellows are activated.

Because a monopolar surgical knife used in ESD cuts tissues laterally, a bending force is applied to the instrument. Consequently, we aimed to measure the bending force applied to the monopolar knife by integrating a monopolar knife to the tip of the 3D force sensor. Hence, the direction of the force can be determined by our force sensor. The proposed 3D force sensor combined with the soft robotic arm was applied to force detection in palpation and tissue dissection in an ex vivo test with chicken breast as shown in Figs. 5c, 5d and supporting video. As a result, the force sensor could detect the force interaction, indicating the potential for this sensor's use in surgical applications through future investigations and development.

IV. Conclusion

In this paper, we have integrated a novel sensing element into a 3D force sensor and demonstrated its application in a surgical system. We have demonstrated the sensing element's ability to tune its sensitivity to applied force, with a sensitivity ranging at least from -6.76 kPa/mm to -23.12 kPa/mm. We applied a NN model to train the sensor's output in response to force, and achieved an x, y, and z-axis accuracy of ~1.0, ~1.3, and ~0.94% respectively. The sensor was able to detect forces larger than 0.1 N, and large forces comparable with similar sensors in the literature. Finally, we showed that the sensor has the potential to be integrated into surgical systems, with force detection demonstrated in palpation and electrocautery procedures.

Acknowledgment

The authors acknowledge support from the UNSW Start-Up Grant (PS58173), the UNSW Scientia Fellowship Grant (PS46197), the Vanguard Grant from the National Heart Foundation of Australia (RG204224), the GROW Early Career Academics Grant (PS66730), and Google Research Scholar Award (PS66591). Mai Thanh Thai, Chi Cong Nguyen, and Trung Thien Hoang would like to acknowledge supports from the Science and Technology Scholarship Program for Overseas Study for Masters and Doctoral Degrees, Vingroup, Vietnam.

References

[1] C. Lee *et al.*, "Soft robot review," *International Journal of Control, Automation and Systems,* vol. 15, no. 1, pp. 3-15, 2017.

[2] G. M. Whitesides, "Soft robotics," *Angewandte Chemie International Edition,* vol. 57, no. 16, pp. 4258-4273, 2018.

[3] D. Rus and M. T. Tolley, "Design, fabrication and control of soft robots," *Nature,* vol. 521, no. 7553, pp. 467-475, 2015.

[4] S. Kim, C. Laschi, and B. Trimmer, "Soft robotics: a bioinspired evolution in robotics," *Trends in Biotechnology,* vol. 31, no. 5, pp. 287-294, 5// 2013, doi: http://dx.doi.org/10.1016/j.tibtech.2013.03.002.

[5] F. Iida and C. Laschi, "Soft robotics: Challenges and perspectives," *Procedia Computer Science,* vol. 7, pp. 99-102, 2011.

[6] C. Tawk and G. Alici, "A Review of 3D-Printable Soft Pneumatic Actuators and Sensors: Research Challenges and Opportunities," *Advanced Intelligent Systems,* vol. 3, no. 6, p. 2000223, 2021.

[7] K. Elgeneidy, N. Lohse, and M. Jackson, "Bending angle prediction and control of soft pneumatic actuators with embedded flex sensors–a data-driven approach," *Mechatronics,* vol. 50, pp. 234-247, 2018.

[8] G. Gerboni, A. Diodato, G. Ciuti, M. Cianchetti, and A. Menciassi, "Feedback control of soft robot actuators via commercial flex bend sensors," *IEEE/ASME Transactions on Mechatronics,* vol. 22, no. 4, pp. 1881-1888, 2017.

[9] J. T. Muth *et al.*, "Embedded 3D printing of strain sensors within highly stretchable elastomers," *Advanced materials,* vol. 26, no. 36, pp. 6307-6312, 2014.

[10] J. C. Yeo, H. K. Yap, W. Xi, Z. Wang, C. H. Yeow, and C. T. Lim, "Flexible and stretchable strain sensing actuator for wearable soft robotic applications," *Advanced Materials Technologies,* vol. 1, no. 3, p. 1600018, 2016.

[11] S. K. Yildiz, R. Mutlu, and G. Alici, "Fabrication and characterisation of highly stretchable elastomeric strain sensors for prosthetic hand applications," *Sensors and Actuators A: Physical,* vol. 247, pp. 514-521, 2016.

[12] R. L. Truby *et al.*, "Soft somatosensitive actuators via embedded 3D printing," *Advanced Materials,* vol. 30, no. 15, p. 1706383, 2018.

[13] Y.-L. Park, B.-R. Chen, and R. J. Wood, "Design and fabrication of soft artificial skin using embedded microchannels and liquid conductors," *IEEE Sensors journal,* vol. 12, no. 8, pp. 2711-2718, 2012.

[14] W. Xi, J. C. Yeo, L. Yu, S. Zhang, and C. T. Lim, "Ultrathin and wearable microtubular epidermal sensor for real-time physiological pulse monitoring," *Advanced Materials Technologies,* vol. 2, no. 5, p. 1700016, 2017.

[15] M. D. Dickey, "Stretchable and soft electronics using liquid metals," *Advanced Materials,* vol. 29, no. 27, p. 1606425, 2017.

[16] K. Elgeneidy, G. Neumann, M. Jackson, and N. Lohse, "Directly printable flexible strain sensors for bending and contact feedback of soft actuators," *Frontiers in Robotics and AI,* vol. 5, p. 2, 2018.

[17] V. Sencadas, R. Mutlu, and G. Alici, "Large area and ultra-thin compliant strain sensors for prosthetic devices," *Sensors and Actuators A: Physical,* vol. 266, pp. 56-64, 2017.

[18] T. N. Do and Y. Visell, "Stretchable, twisted conductive microtubules for wearable computing, robotics, electronics, and healthcare," *Scientific reports,* vol. 7, no. 1, pp. 1-12, 2017.

[19] O. Atalay, A. Atalay, J. Gafford, and C. Walsh, "A highly sensitive capacitive-based soft pressure sensor based on a conductive fabric and a microporous dielectric layer," *Advanced materials technologies,* vol. 3, no. 1, p. 1700237, 2018.

[20] L. Viry *et al.*, "Flexible three-axial force sensor for soft and highly sensitive artificial touch," *Advanced materials,* vol. 26, no. 17, pp. 2659-2664, 2014.

[21] B. Li, Y. Gao, A. Fontecchio, and Y. Visell, "Soft capacitive tactile sensing arrays fabricated via direct filament casting," *Smart*

Materials and Structures, vol. 25, no. 7, p. 075009, 2016. [Online]. Available: http://stacks.iop.org/0964-1726/25/i=7/a=075009.

[22] A. Frutiger *et al.*, "Capacitive soft strain sensors via multicore–shell fiber printing," *Advanced Materials,* vol. 27, no. 15, pp. 2440-2446, 2015.

[23] H. Yang, Y. Chen, Y. Sun, and L. Hao, "A novel pneumatic soft sensor for measuring contact force and curvature of a soft gripper," *Sensors and Actuators A: Physical,* vol. 266, pp. 318-327, 2017.

[24] C. Tawk, M. in het Panhuis, G. M. Spinks, and G. Alici, "Soft pneumatic sensing chambers for generic and interactive human–machine interfaces," *Advanced Intelligent Systems,* vol. 1, no. 1, p. 1900002, 2019.

[25] C. Tawk, E. Sariyildiz, H. Zhou, M. in het Panhuis, G. M. Spinks, and G. Alici, "Position control of a 3D printed soft finger with integrated soft pneumatic sensing chambers," in *2020 3rd IEEE International Conference on Soft Robotics (RoboSoft)*, 2020: IEEE, pp. 446-451.

[26] K. Kong and M. Tomizuka, "A gait monitoring system based on air pressure sensors embedded in a shoe," *IEEE/ASME Transactions on mechatronics,* vol. 14, no. 3, pp. 358-370, 2009.

[27] H. Choi, P.-G. Jung, K. Jung, and K. Kong, "Design and fabrication of a soft three-axis force sensor based on radially symmetric pneumatic chambers," in *2017 IEEE International Conference on Robotics and Automation (ICRA)*, 2017: IEEE, pp. 5519-5524.

[28] D. Gong, R. He, J. Yu, and G. Zuo, "A pneumatic tactile sensor for co-operative robots," *Sensors,* vol. 17, no. 11, p. 2592, 2017.

[29] R. Slyper and J. Hodgins, "Prototyping robot appearance, movement, and interactions using flexible 3d printing and air pressure sensors," in *2012 IEEE RO-MAN: The 21st IEEE International Symposium on Robot and Human Interactive Communication*, 2012: IEEE, pp. 6-11.

[30] M. Vázquez, E. Brockmeyer, R. Desai, C. Harrison, and S. E. Hudson, "3d printing pneumatic device controls with variable activation force capabilities," in *Proceedings of the 33rd Annual ACM Conference on Human Factors in Computing Systems*, 2015, pp. 1295-1304.

[31] D. S. Chathuranga, Z. Wang, Y. Noh, T. Nanayakkara, and S. Hirai, "A soft three axis force sensor useful for robot grippers," in *2016 IEEE/RSJ International Conference on Intelligent Robots and Systems (IROS)*, 2016: IEEE, pp. 5556-5563.

[32] D. M. Vogt, Y.-L. Park, and R. J. Wood, "Design and characterization of a soft multi-axis force sensor using embedded microfluidic channels," *IEEE sensors Journal,* vol. 13, no. 10, pp. 4056-4064, 2013.

[33] P. Yu, W. Liu, C. Gu, X. Cheng, and X. Fu, "Flexible piezoelectric tactile sensor array for dynamic three-axis force measurement," *Sensors,* vol. 16, no. 6, p. 819, 2016.

[34] L. He, N. Herzig, T. Nanayakkara, and P. Maiolino, "3D-Printed Soft Sensors for Adaptive Sensing with Online and Offline Tunable Stiffness," *Soft Robotics,* 2022.

[35] M. M. Sadeghi, K. Dowling, R. L. Peterson, and K. Najafi, "High sensitivity, high density micro-hydraulic force sensor array utilizing stereo-lithography fabrication technique," in *2013 IEEE 26th International Conference on Micro Electro Mechanical Systems (MEMS)*, 2013: IEEE, pp. 673-676.

[36] T. Sasaki, Y. Fujiwara, K. Tachikawa, K. Terabayashi, and K. Dohda, "Hydraulic micro device with force sensing for measurement of mechanical characteristics," *International Journal of Automation Technology,* vol. 14, no. 4, pp. 625-632, 2020.

[37] M. A. Meller, M. Bryant, and E. Garcia, "Reconsidering the McKibben muscle: Energetics, operating fluid, and bladder material," *Journal of Intelligent Material Systems and Structures,* vol. 25, no. 18, pp. 2276-2293, 2014.

[38] M. De Volder and D. Reynaerts, "Pneumatic and hydraulic microactuators: a review," *Journal of Micromechanics and microengineering,* vol. 20, no. 4, p. 043001, 2010.

[39] M. Focchi *et al.*, "Water/air performance analysis of a fluidic muscle," in *2010 IEEE/RSJ international conference on intelligent robots and systems*, 2010: IEEE, pp. 2194-2199.

[40] D. G. Caldwell, G. A. Medrano-Cerda, and M. Goodwin, "Control of pneumatic muscle actuators," *IEEE Control Systems Magazine,* vol. 15, no. 1, pp. 40-48, 1995.

[41] R. Tiwari, M. A. Meller, K. B. Wajcs, C. Moses, I. Reveles, and E. Garcia, "Hydraulic artificial muscles," *Journal of Intelligent Material Systems and Structures,* vol. 23, no. 3, pp. 301-312, 2012.

[42] M. T. Thai, P. T. Phan, T. T. Hoang, H. Low, N. H. Lovell, and T. N. Do, "Design, Fabrication, and Hysteresis Modeling of Soft Microtubule Artificial Muscle (SMAM) for Medical Applications," *IEEE Robotics and Automation Letters,* vol. 6, no. 3, pp. 5089-5096, 2021.

[43] P. T. Phan, M. T. Thai, T. T. Hoang, N. H. Lovell, and T. N. Do, "HFAM: soft hydraulic filament artificial muscles for flexible robotic applications," *Ieee Access,* vol. 8, pp. 226637-226652, 2020.

[44] K. Chin, T. Hellebrekers, and C. Majidi, "Machine learning for soft robotic sensing and control," *Advanced Intelligent Systems,* vol. 2, no. 6, p. 1900171, 2020.

[45] M. T. Thai, P. T. Phan, T. T. Hoang, S. Wong, N. H. Lovell, and T. N. Do, "Advanced intelligent systems for surgical robotics," *Advanced Intelligent Systems,* vol. 2, no. 8, p. 1900138, 2020.